УДК 551.556.8

© *K. V. Fokina**, *K. Yu. Bulgakov*, 2022
Shirshov Institute of Oceanology, Russian Academy of Sciences, 117997, Nahimovskiy prospekt, 36, Moscow, Russia
*E-mail: fokinakarina@yandex.ru

COUPLED MODELLING OF WIND WAVES AND WAVE BOUNDARY LAYER

Received 13.09.2021, revised 29.10.2021, accepted 25.11.2021

The coupled wind-wave model is considered. The model includes two components: the 1-D wave boundary layer model and the 2-D wave model. The coupled model is used in two versions: in the presence and the absence of the wave produced momentum flux. A series of experiments was performed for different external parameters: wind speed at the upper boundary of the wave boundary layer and the inverse wave age. The vertical profiles of wind velocity, turbulent and wave produced momentum fluxes were studied and compared to the results obtained from the wave boundary layer model. The comparison showed that the results of coupled modeling coincide exactly with the results from the wave boundary layer model in the case of fully developed waves and differ significantly if developing waves are considered. It is demonstrated that wave produced momentum flux produces considerable deviations of the wind velocity profile in the lower part of the wave boundary layer from the logarithmic profile.

Keywords: wave boundary layer, wind waves, wave produced momentum flux, wave spectrum, ocean-atmosphere interaction

© *К. В. Фокина**, *К. Ю. Булгаков*, 2022
Институт океанологии им. П.П. Ширшова РАН, 117997, Нахимовский пр., д. 36, г. Москва, Россия
*E-mail: fokinakarina@yandex.ru

СОВМЕСТНОЕ МОДЕЛИРОВАНИЕ ВЕТРОВЫХ ВОЛН И ВОЛНОВОГО ПОГРАНИЧНОГО СЛОЯ

Статья поступила в редакцию 13.09.2021, после доработки 29.10.2021, принята к печати 25.11.2021

Сформулирована и реализована совместная модель волнового пограничного слоя и волн, объединяющая разработанные ранее соответствующие модели. Совместная модель использовалась в двух вариантах: с учетом и без учета волнового потока импульса. Проведены серии экспериментов с широким диапазоном изменения входных параметров (скорость ветра на верхней границе волнового пограничного слоя и обратный возраст волны) и рассчитаны значения метеорологических характеристик: скорости ветра, волнового и турбулентного потоков импульса в волновом пограничном слое. Полученные результаты проанализированы с целью продемонстрировать необходимость учета волнового потока импульса в моделях волнового пограничного слоя, а также показать особенности результатов совместного моделирования для описания волнового пограничного слоя. Показано, что результаты совместного моделирования для указанных метеорологических характеристик значительным образом отличаются от результатов, полученных по модели волнового пограничного слоя, для развитого и слаборазвитого волнения. Учет волнового потока импульса приводит к заметным отклонениям профиля скорости ветра в нижней части волнового пограничного слоя от логарифмического, применимого при описании атмосферного пограничного слоя.

Ключевые слова: волновой пограничный слой, ветровые волны, волновой поток импульса, волновой спектр, взаимодействие океана и атмосферы

1. Introduction

The theory of the boundary layer was developed in detail in the work of S.S. Zilitinkevich [1]. This paper presents the results of a study of the lower part of the atmospheric boundary layer above the sea. The wave boundary layer (further referred to as 'WBL') is an integral element of the planetary boundary layer in which an exchange of momentum between the atmosphere and the ocean is formed.

An understanding of the wind-waves interactions is important for many applications: wave forecasting models, weather forecasting, and climate modeling. Specifics of boundary layer above sea is a presence of the wave-induced velocity and pressure fields. The wave boundary layer is considered as the lowest part of the atmospheric boundary

Ссылка для цитирования: *Фокина К.В.*, *Булгаков К.Ю.* Совместное моделирование ветровых волн и волнового пограничного слоя // Фундаментальная и прикладная гидрофизика. 2022. Т. 15, № 1. С. 73–81. doi: 10.48612/fpg/4pg1-agtu-u56k
For citation: *Fokina K.V.*, *Bulgakov K. Yu*. Coupled Modelling of Wind Waves and Wave Boundary Layer. *Fundamental and Applied Hydrophysics*. 2022, 15, 1, 73–81. doi: 10.48612/fpg/4pg1-agtu-u56k

layer with thickness of several meters, where fluctuations caused by waves are clearly pronounced [2]. The height of WBL is the order of significant wave height. The motion within the WBL is affected by the surface waves, which means its structure depends on the characteristics of the wave field. Since the WBL forms wave stress, its structure influences the dynamics of the entire atmospheric boundary layer. The stress is composed of two main components: the turbulent momentum flux and the wave produced momentum flux (WPMF), which transfers energy and momentum to waves [3, 4]. The stationary structure of the wave boundary layer is defined by wind velocity (or horizontal stress) at upper level and by spectral shape of wind waves. Hence the WBL and wave field form the closely connected dynamic system, which should be considered as a single object for modeling.

The two-dimensional coupled model of the wave boundary layer and potential waves is described in [5]. The airflow is described with Reynolds equation with parameterized turbulence. The waves are simulated by conformal model [6]. The air and wave components of the model were coupled at each time step by transferring the surface pressure obtained in the WBL model to the wave model; the shape of the surface and the components of the surface velocity, obtained in the wave model in the WBL model. Last version of the coupled model [7] is capable of introducing an explicit description of the physics of the wind–wave interactions in the wave forecasting models.

The present work continues the studies of the wave boundary layer and the wind waves interactions by coupling with one-dimensional WBL model. 2-D WBL model is much more detailed than 1-D model, but 2-D computations take considerable computer resources. That is why 2-D WBL model can be used for investigation of the WBL physics but not for wave forecasting of coupled ocean-atmosphere models. The main advantage of 1-D model is sharp acceleration of computations. Thus, such model can be implemented in wave forecasting models in the future.

2. The one-dimensional wave boundary layer model

The one-dimensional WBL model presented in [8, 9] is intended to describe the structure and evolution of the wave boundary layer and for use in ocean–atmosphere coupled models. The equations of the one-dimensional WBL model were obtained in [7] by averaging the two-dimensional Reynolds equations of motion written in the conformal coordinate system along the horizontal coordinate lines:

$$\frac{\partial u}{\partial t} = \frac{\partial}{\partial z}\left(K\frac{\partial u}{\partial z} + \tau_w \right), \tag{1}$$

$$\frac{\partial e}{\partial t} = \frac{\partial}{\partial z} K\frac{\partial e}{\partial z} + P - \varepsilon, \tag{2}$$

where u is the horizontal component of the velocity, τ_w is the wave induced momentum flux, e is the turbulence kinetic energy, ε is the dissipation rate:

$$\varepsilon = \frac{\sqrt[3]{e / C_1}}{\kappa z}. \tag{3}$$

where $C_1 = 3.7$; κ is a *von Karman constant*.
K is a turbulent coefficient:

$$K = \kappa z\sqrt{e / C_1}, \tag{4}$$

P is a rate of turbulent energy production:

$$P = \frac{\partial u}{\partial z}\left(K\frac{\partial u}{\partial z} + \tau_w \right). \tag{5}$$

The Eqs. (1, 2, 5) differ from routine boundary layer equation by presence of effects connected with wave-produced momentum flux τ_w (WPMF). The equations are approximated on a non-uniform grid $\Delta z_{i+1} = \gamma_z \Delta z_i$, where $\gamma_z = 1.10$ is the stretching coefficient. The domain height is equal to 10 meters with the number of vertical levels $L = 50$.

As shown in [7], the averaged profiles of the spectral components of the WPMF considerably depend on the wavenumber k. Normalizing each profile by its surface values of $\tau^k_{w_0}$ and introducing the non-dimensional wave height kz, the profiles converge and τ^k_w can be described as follows

$$\tau^k_w = \tau^k_{w0} \exp(Gkz), \tag{6}$$

where G is the weak function of $\bar{\omega} = \Omega / \Omega_p$

$$G = 0.985 + 0.4(\bar{\omega})^{0.81}, \tag{7}$$

where Ω_p is the non-dimensional frequency in the spectral peak, Ω is the non-dimensional frequency, calculated by the formula

$$\Omega_k = \omega_k U(\lambda_k/2)/g, \tag{8}$$

where $\omega_k = |gk|^{1/2}$, U is wind speed at the height $\lambda_k/2$.

The Fourier component of the WPMF on the surface τ_{w0}^k is defined through the following expression

$$\tau_{w0}^k = kg\beta_{-k}(\overline{\Omega}_k)S(k), \tag{9}$$

where β is the imaginary part of beta function, S is the one-dimensional wave spectrum.

Thus, the WPMF profile $\tau_w(m^2/s^2)$, included in equations (1) and (5), is calculated by the relation [7]:

$$\tau_w(z) = \sum_{i=0}^{M-1} \omega_i^2 \beta(\Omega_i) S(\omega_i) \exp\left(-G\left(\omega_i \frac{\omega_i^2 z}{g}\right)\Delta\omega_i\right), \tag{10}$$

where M is the wave number.

Approximation of the imaginary part of β-function is obtained from [9]:

$$\beta_{-k} = \begin{cases} \beta_0 + a_0(\Omega - \Omega_0) + a_1(\Omega - \Omega_0)^2 & \Omega_0 < \Omega \\ \beta_0 + a_0(\Omega - \Omega_0) - a_1(\Omega - \Omega_0)^2 & \Omega_0 > \Omega \end{cases}, \tag{11}$$

where $a_0 = 0.02277$, $a_1 = 0.09476$, $\beta_0 = -0.02$, $\Omega_0 = 0.58$.

Equation (10) assumes that WPMF is a linear composition of fluxes produced by wave modes which surface values are calculated with a use of β-function. Each spectral component of WPMF decreases with height exponentially. To compute the energy input at each interval $\Delta\omega_i$, it is necessary to calculate the wind speed at a height equal to half of the wavelength l/2. Such multiple calculations take a lot of computer time. This problem is solved by introducing the approximation of wind speed profile using the cubic spline interpolation. The spline coefficients were calculated based on the tridiagonal *matrix* method. After that the wind velocity at reference levels is calculated analytically with no use of interpolation procedure.

For equation (1), the wind speed U_{10} is set at the upper boundary. The surface stress is assigned in a form

$$\left(K\frac{du}{dz}\right)_{z=0} = v_{0*}^2, \tag{12}$$

where the near-wall value of the friction velocity v_{0*} is calculated by the formula:

$$v_{0*} = \kappa U_1 \left(\ln\frac{z}{z_{00}}\right)^{-1}. \tag{13}$$

Where z_{00} is a roughness parameter calculated by the formula from [10]

$$z_{00} = 0{,}11\frac{\eta}{v_*}, \tag{14}$$

where v_* is friction velocity, η is the viscosity coefficient ($1.5\cdot10^{-5}$ m^2/s). Scheme (12)–(14) assumes the vertical resolution in a vicinity of surface is so high that lower level falls in viscous sublayer. For equation (2), the upper value of the turbulence energy e is equal to:

$$e_{z=H} = C_1 v_*^2, \tag{15}$$

where

$$v_*^2 = \left(K\frac{\partial u}{\partial z}\right)_{z=H}. \tag{16}$$

The diffusion of turbulent energy at wave surface is equal to zero:

$$\left(K_e\frac{de}{dz}\right)_{z=0} = 0. \tag{17}$$

The initial conditions are the profiles of wind speed $U(z)$, turbulence energy $e(z)$, and dissipation rate $\varepsilon(z)$:

$$U(z) = \frac{v_*}{\kappa}\ln\frac{z}{z_{00}};\ \ e(z) = C_1 v_*^2;\ \ \varepsilon(z) = \frac{v_*^3}{\kappa z}. \tag{18}$$

3. The wave model equations

The process of wave dynamics is reproduced using the one-dimensional nonlinear model [6], which includes parametrizations for energy input and wave breaking and allows to consider nonlinear effects on the time scales much longer than the wave period. Periodic one-dimensional waves are considered. The principal equations for waves written in Cartesian coordinates, are Laplace equation for the velocity potential Φ

$$\Phi_{xx} + \Phi_{zz} = 0 \tag{19}$$

the kinematic condition at free surface $z = h(x, t)$

$$h_t + h_x\Phi_x - \Phi_z = 0 \tag{20}$$

and the Lagrange integral

$$\Phi_\tau + \frac{1}{2}\left(\Phi_x^2 + \Phi_z^2\right) + h + p_0 = 0, \tag{21}$$

where p_0 is the surface pressure.

The equations are solved in the domain

$$-\infty < x < \infty \; -H < z < h(x, t). \tag{22}$$

Since numerical integration of system (19)–(21) is computationally inefficient, to make a numerical solution feasible, the surface-following coordinate system is introduced. The use of such coordinates allows simplifications in the formulation of the numerical scheme. The new coordinate system maps the domain (22) onto the strip

$$-\infty < \xi < \infty \; -H < \xi < 0 \tag{23}$$

with periodicity condition

$$x(\xi, \zeta, \tau) = x(\xi + 2\pi, \zeta, \tau) + 2\pi, \tag{24}$$

$$z(\xi, \zeta, \tau) = z(\xi + 2\pi, \zeta, \tau), \tag{25}$$

where τ is the new time coordinate.

Conformal mapping, due to periodicity condition (24)–(25), can be represented as:

$$x = \xi + x_0(\tau) + \sum_{-M\le k\le M, k\neq 0} \eta_{-k}(\tau)\frac{\cosh k(\zeta + H)}{\sinh kH}\vartheta_k(\xi), \tag{26}$$

$$z = \zeta + \eta_0(\tau) + \sum_{-M\le k\le M, k\neq 0} \eta_k(\tau)\frac{\sinh k(\zeta + H)}{\sinh kH}\vartheta_k(\xi). \tag{27}$$

Due to conformal mapping, Laplace equation retains its shape and can be solved analytically. The system (19)–(21) is written in the new coordinates as

$$\Phi_{\xi\xi} + \Phi_{\varsigma\varsigma} = 0, \tag{28}$$

$$z_\tau = x_\xi\xi_\tau + z_\xi\varsigma_\tau, \tag{29}$$

and the Lagrange integral

$$\Phi_\tau + \zeta\Phi_\xi + \frac{1}{2}J^{-1}\left(\Phi_\xi^2 - \Phi_\zeta^2\right) + z + p_0 = 0, \tag{30}$$

where J is the Jacobian of mapping:

$$J = x_\xi^2 + z_\xi^2 = x_\zeta^2 + z_\zeta^2. \tag{31}$$

The boundary condition requires attenuation of the vertical velocity at depth:

$$\hat{O}_\zeta(\xi, \zeta \to \infty, \tau) = 0. \tag{32}$$

The Laplace equation (28) along with (32) is solved through the Fourier expansion, which reduces (28)–(30) to a 1-D problem:

$$\Phi = \sum_{-M\le k\le M} \varphi_k(\tau)\exp(k\zeta)\vartheta_k(\xi), \tag{33}$$

where φ_k are the Fourier coefficients of the surface potential $\Phi(\xi, \zeta = 0, \tau)$, ϑ_k are the basic functions:

$$\vartheta_k(\xi) = \begin{cases} \cos k\xi, k \geq 0 \\ \sin k\xi, k < 0 \end{cases}. \tag{34}$$

The wind–waves energy and momentum exchange occurs due to the dynamic surface pressure p_0, which is included in equation (30). According to linear theory [11], the Fourier components of the surface pressure p_0 are related to the components of the surface elevation by the following expression:

$$p_{k,l} + ip_{-k,-l} = \left(\beta_{k,l} + i\beta_{-k,-l}\right)\left(h_{k,l} + ih_{-k,-l}\right), \tag{35}$$

where β_k and β_{-k} are real and imaginary parts of β-function.

Equations of the wave model, as well as equations for the WBL, are written in a non-dimensional form with the following scales: length L and time $T = L^{1/2}g^{-1/2}$ (g is the gravity acceleration). Equations (28)–(31) constitute a closed system of predictive equations for surface functions $z(\xi, \zeta = 0, \tau) = \eta(\xi, \tau)$ и $\Phi(\xi, \zeta = 0, \tau)$, which can be solved using the Fourier transformation.

4. Coupling of the wave model with the model of the wave boundary layer

The coupled model allows to directly connect the dynamics of the boundary layer with the wave spectrum. The wave spectrum in the WBL model is set as the initial conditions, has a smoother idealized shape, does not evolve in the course of the calculations, and differs significantly from the spectrum simulated by the wave model that is closer to the real spectrum. The main difference is that simulated waves obtain the nonlinear features: the wave crests are sharper and troughs are smoother than in the initially assigned field.

The coupling process is reduced to a two-way exchange of fields between the models, which makes it possible to consider the mutual influence of wind waves and the atmosphere r. Thus, both models are integrated simultaneously, exchanging matching information: the wave model provides the WBL model with wave spectrum, which is subsequently used to calculate the WPMF produced by the waves (10). The development of the wave field occurs under the influence of energy input, dissipation, and nonlinear interaction between wind and waves. In this case, as noted earlier, energy input is carried out due to changes in the surface pressure. The use of the approximation for β function (11) and the wind speed profile calculated in the WBL model allows obtaining the values of the surface pressure determined by equation (30).

5. Calculations and results

The wave spectrum is approximated with the number of modes $M = 2048$ and the number of grid nodes $N = 8192$. The experiments were performed for the values of the inverse wave age $\Omega_n = \{0.855, 1, 2, 3, 4, 5, 6, 7, 8, 9, 10\}$ and the wind speed at the upper boundary of the WBL $U_{10} = \{10, 20, 30\}$ m/s. The non-dimensional wind speed at the upper boundary is determined by the ratio:

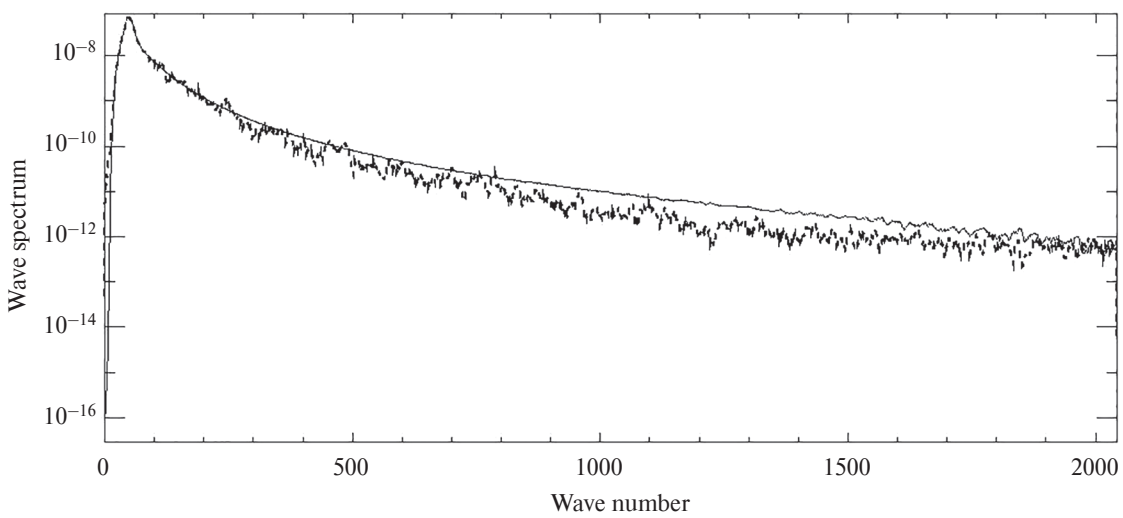

Fig. 1. The wave spectrum obtained by the WBL model (solid line) and the wave model (dashed line)

$$U_n = \frac{\Omega_n}{\sqrt{k_p}}, \tag{36}$$

where $k_p = 50$ is the peak wave number.

The time step Δt is equal to 0.0025. The length scale $L = U_{10}/U_n$ is determined from the calculated non-dimensional wind speed and the given value of the dimensional wind speed. The wave spectrum for each group of experiments is assigned by the JONSWAP spectrum [12]:

$$S(\omega) = \alpha g^2 \omega^{-5} \exp\left(-1{,}25\tilde{\omega}^{-4}\right)\gamma^{\Gamma}, \tag{37}$$

where $\tilde{\omega} = \omega / \omega_p$ ($\omega_p = \dfrac{\Omega_0 g}{U_{10}}$ — frequency at spectral peak), $\gamma = 3.3$, $\alpha = 0.01(U_{10}/C_p)^{0.66}$, $\Gamma = \exp\left(\left(\dfrac{\tilde{\omega}-1}{\sqrt{2}\sigma}\right)^2\right)$.

Three versions of the model are considered: 1) one-dimensional model of the wave boundary layer; 2) coupled model including the WPMF (taking into account the deviation of the wind profile from the logarithmic profile); 3) coupled model not taking into account the WPMF, i.e. considering a logarithmic wind profile.

The profiles of the turbulent τ_t and wave τ_w momentum fluxes obtained by the WBL model and the coupled model for the wind speed at the WBL upper boundary equal to 10, 20, and 30 m/s and the extreme values of the inverse wave age: fully developed conditions ($\Omega_n = 0.855$) and young waves ($\Omega_n = 10$) are shown in Fig. 2. Each run was performed until the full momentum flux became constant over height.

As seen, the decrease in turbulent momentum flux at approaching the surface is compensated by the increase in the WPMF. In the case of fully developed waves, the differences of momentum fluxes values calculated with the coupled model and single WBL model are not observed over the entire WBL height for all U_{10} values. For younger sea, the difference in momentum fluxes for the two types of considered experiments is clearly manifested. Thus, for $\Omega_n = 10$, the values of τ_w on the surface obtained using the coupled model are, on average, by 30 % less than the values obtained using the WBL model, since the parameterization of the WPMF includes the value of the wave spectrum, which, as has been illustrated earlier, show noticeable differences for the WBL model and the wave model. In a steady boundary layer the total momentum flux is constant over height; hence, the differences in the vertical WPMF profiles should be reflected in the vertical turbulent flux profiles. Thus, the maximum distinctions of the turbulent fluxes values are observed at the upper boundary of the domain in each experiment.

As shown in the Fig. 3 (*a*, *b*) for $U_{10} = 10$ m/s and $\Omega_n \le 4$ the WPMF values near the surface can exceed the values of the turbulent flux by 15–20 % when using the coupled model; whereas for the WBL model the WPMF values are less than the turbulent flux values irrespective of the inverse wave age and wind speed.

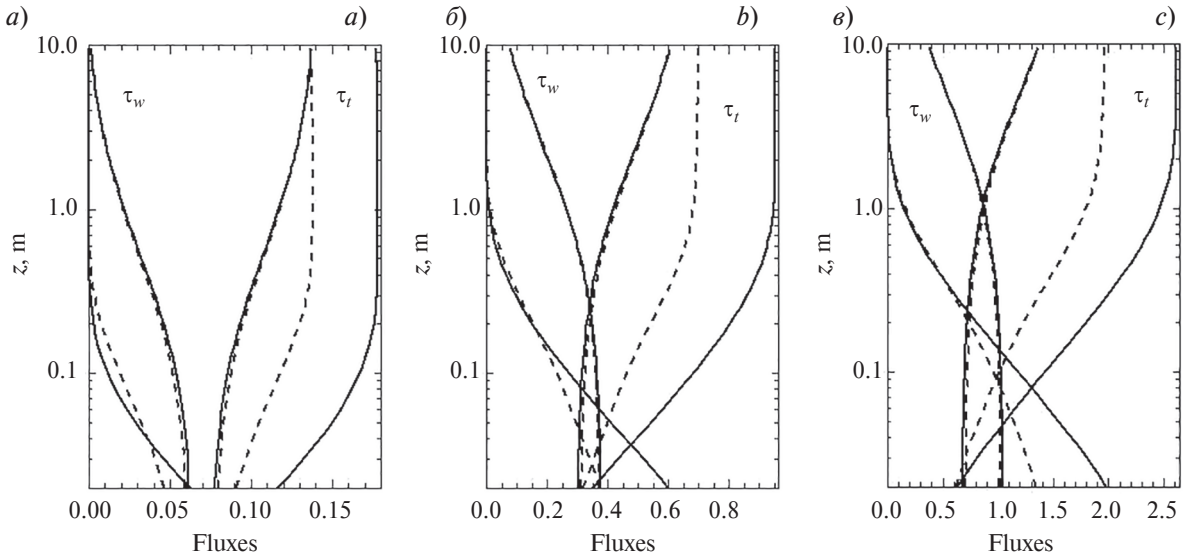

Fig. 2. The turbulent τ_t (curves on the right) and wave τ_w (curves on the left) momentum fluxes profiles (solid curves — the WBL model, dashed curves — coupled model) for extreme values of $\Omega_n = 0.855$ and 10: *a* — $U_{10} = 10$ m/s; *b* — $U_{10} = 20$ m/s; *c* — $U_{10} = 30$ m/s

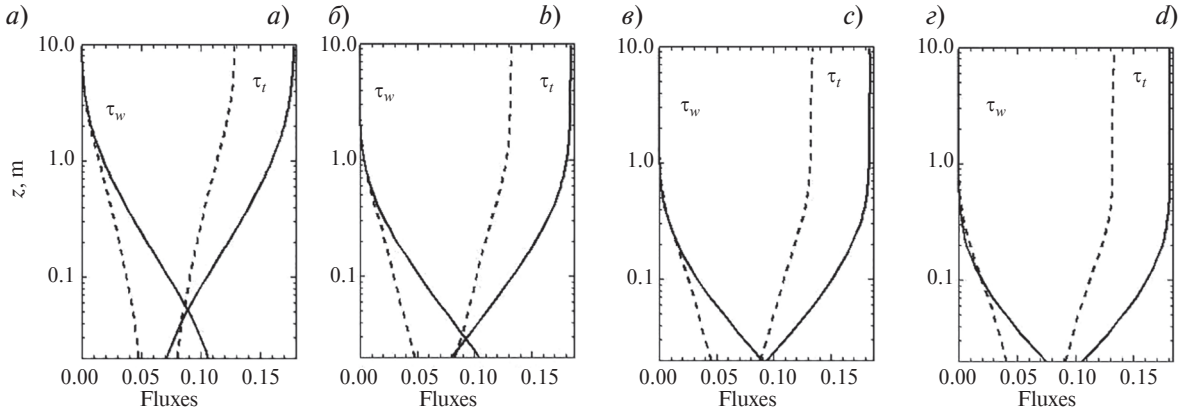

Fig. 3. The turbulent τ_t and wave τ_w momentum fluxes profiles for U_{10} = 10 m/s (solid curves — the WBL model, dashed curves — coupled model): *a* — Ω_n = 2; *b* — Ω_n = 4; *c* — Ω_n = 6; *d* — Ω_n = 8

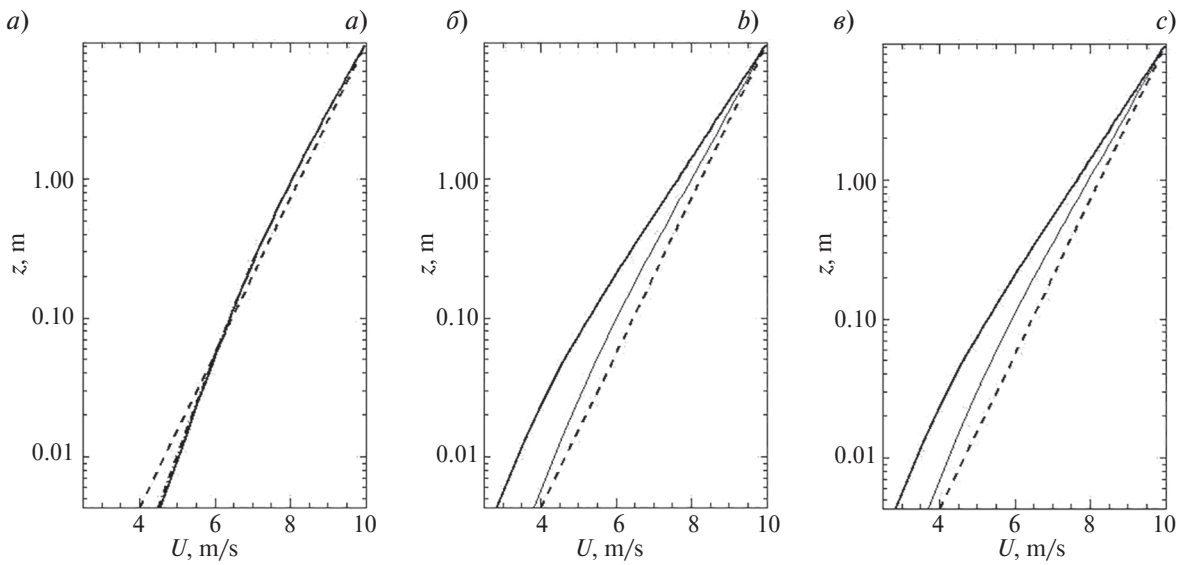

Fig. 4. Velocity *u* profiles for U_{10} = 10 m/s (thick solid curves — the WBL model, thin solid curves — the coupled model, dashed curves — the coupled model without the WPMF): *a* — Ω_n = 0.855; *b* — Ω_n = 4; *c* — Ω_n = 8

The wind speed profiles for different values of the inverse wave age for three values of wind speed (10, 20, and 30 m/s) are shown in Fig. 4 and Fig. 5 as a function of height *z*(m). The dotted line corresponds to the logarithmic wind profile, i.e. shows the wind profile in the absence of the WPMF. The results of coupled modeling for Ω_n = 0.855 completely coincide with the results obtained by the WBL model. Deviations from the logarithmic profile in the lower part of the WBL are observed, and the magnitude of this deviation becomes larger with the increase in U_{10}. As the inverse wave age increases, the wind profiles calculated by the two models show slight deviation through the entire WBL height (Fig. 4, *b*, *c*).

The wind velocity profiles obtained from the coupled model for U_{10} = 20 m/s and 30 m/s and all the values of Ω_n (Fig. 5, *a*, *c*) demonstrate smaller scatter of the wind speed values compared to the ones obtained from the WBL model. The deviations from the WBL model reach 2–3 m/s in the lower part of the domain for large values of the inverse wave age.

As seen, in the lowest part of the WBL, deviations of the wind velocity profile from the logarithmic profile reach several meters at U_{10} = 10 m/s, 5 m/s at U_{10} = 20 m/s, and at U_{10} = 30 m/s — about 10 m/s. It is also worth assuming that the use of the coupled model will mainly affect the results for developing and underdeveloped waves (in the present work — for the values of Ω_n being in the range from 2 to 10).

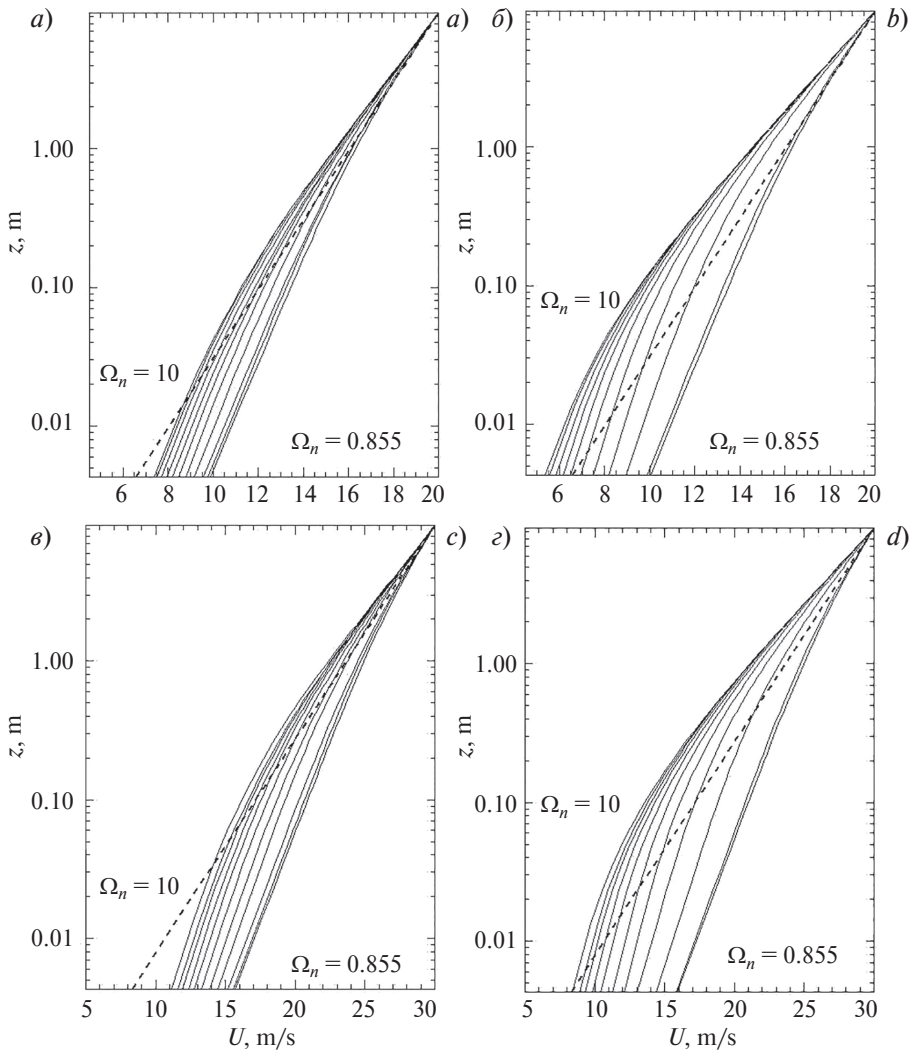

Fig. 5. Velocity *u* profiles: *a* — the coupled model for U_{10} = 20 m/s; *b* —the WBL model for U_{10} = 20 m/s; *c* — the coupled model for U_{10} = 30 m/s; *d* — the WBL model for U_{10} = 30 m/s. The dotted line refers to profile in absence of wave produced momentum flux. In each group, the curves are in order of growing Ω_n (from left to right)

6. Conclusion

The results confirm that coupled modeling of the WBL and waves dynamics does not give qualitatively new results for fully developed waves (Ω_n = 0.855 and 1). However, for underdeveloped waves (for three presented experiments this refers to the cases when $2 \le \Omega_n \le 10$), the results of the coupled modeling show some peculiarities in comparison to the WBL model: in particular, values of the wind speed, WPMF, and turbulent fluxes obtained as a result of simulations with the WBL model exceed the results of coupled modeling to varying degrees.

The existing WBL models, as a rule, do not consider the division of the total momentum flux into the wave and turbulent components. The illustrated results demonstrate that including the WPMF in the WBL models results in significant deviations of the wind velocity profile from the logarithmic one, and as the wind speed at the upper boundary of the WBL increases, such differences become more distinct, reaching the difference of 40–50 % near the surface. Such deviations appear at all specified values of the inverse wave age. It can be assumed that the inclusion of parameterizations of the WPMF in wave forecasting models can improve the quality of wind waves forecasting. Note that specific feature of WBL can be reproduced at high resolution of wave spectrum and high vertical resolution.

It was shown that the distribution of surface pressure depends on the shape of so-called β-function. It was clearly shown in [13] that the values of β-function obtained from different approximations differ by several times. Note that

the existing uncertainty in β-function shape may significantly influence the results. The thorough investigation of β-function shape is performed in [7], however the results depend on the WBL resolution and such dependence is not clearly described. That means the problem is far from being solved and further investigations of β-function with high-resolution coupled model are highly required.

7. Funding

The presented results were obtained within the framework of the state program No FMWE-2021-0014.

References

1. *Zilitinkevich S.S.* Atmospheric turbulence and planetary boundary layers. *Moscow*, *Fizmatlit*, 2013. 248 p. (in Russian).
2. *Chalikov D.V.* Numerical simulation of the boundary layer above waves. *Boundary-Layer Meteorology*. 1986, 34, 63–98. doi: 10.1007/BF00120909
3. *Hristov T.*, *Friehe C.*, *Miller S.* Wave-coherent fields in air flow over ocean waves: Identification of cooperative behavior buried in turbulence. *Physical Review Letters*. 1998, 81(23), 5245–5248. doi: 10.1103/PhysRevLett.81.5245
4. *Hristov T., Miller S., Friehe C.* Dynamical coupling of wind and ocean waves through wave-induced air flow. *Nature*. 2003, 422(6927), 55–58.
5. *Chalikov D.V.* The numerical simulation of wind — waves interaction. *Journal of Fluid Mechanics*. 1978, 87, 561–582. doi: 10.1017/S0022112078001767
6. *Chalikov D.*, *Sheinin D.* Numerical modeling of surface waves based on principal equations of potential wave dynamics. *Technical Note*. 1996, 64 p.
7. *Chalikov D.*, *Rainchik S.* Coupled numerical modeling of wind and waves and the theory of the wave boundary layer. *Boundary-Layer Meteorology*. 2011, 138, 1–41. doi: 10.1007/s10546-010-9543-7
8. *Chalikov D.V.*, *Bulgakov K. Yu.* The structure of surface layer above sea. *Fundamental and Applied Hydrophysics*. 2019, 12, 2, 50–65 (in Russian). doi: 10.7868/S2073667319020072
9. *Chalikov D.*, *Babanin A.V.* Parameterization of wave boundary layer. *Atmosphere*. 2019, 10, 11, 686. doi: 10.3390/atmos10110686
10. *Monin A.S.*, *Yaglom A.M.* Statistical fluid mechanics: mechanics of turbulence. *Cambridge*, *M.I.T. Press.*, 1971. 770 p. doi: 10.1119/1.10870
11. *Miles J.W.* On the generation of surface waves by shearflows. *Journal of Fluid Mechanics*. 1957, 3, 2, 185–204.
12. *Hasselmann K.*, *Barnett R.P.*, *Bouws E.* Measurements of wind-wave growth and swell decay during the Joint Sea Wave Project (JONSWAP). *Deutsches Hydrogr. Inst*. 1973, 95 p.

Литература

1. *Зилитинкевич С.С.* Атмосферная турбулентность и планетарные пограничные слои. Москва: Физматлит, 2013. 248 с.
2. *Chalikov D.V.* Numerical simulation of the boundary layer above waves // Boundary-Layer Meteorology. 1986. Vol. 34. P. 63–98. doi: 10.1007/BF00120909
3. *Hristov T.*, *Friehe C.*, *Miller S.* Wave-coherent fields in air flow over ocean waves: Identification of cooperative behavior buried in turbulence // Physical Review Letters. 1998. Vol. 81(23). P. 5245–5248. doi: 10.1103/PhysRevLett.81.5245
4. *Hristov T.*, *Miller S.*, *Friehe C.* Dynamical coupling of wind and ocean waves through wave-induced air flow // Nature. 2003. Vol. 422(6927). P. 55–58.
5. *Chalikov D.V.* The numerical simulation of wind — waves interaction // Journal of Fluid Mechanics. 1978. Vol. 87. P. 561–582. doi: 10.1017/S0022112078001767
6. *Chalikov D.*, *Sheinin D.* Numerical modeling of surface waves based on principal equations of potential wave dynamics // Technical Note. 1996. 64 p.
7. *Chalikov D.*, *Rainchik S.* Coupled numerical modeling of wind and waves and the theory of the wave boundary layer // Boundary-Layer Meteorology. 2011. Vol. 138. P. 1–41. doi: 10.1007/s10546-010-9543-7
8. *Чаликов Д.В.*, *Булгаков К.Ю.* Структура приводного слоя атмосферы // Фундаментальная и прикладная гидрофизика. 2019. Т. 12, № 2. С. 50–65. doi: 10.7868/S2073667319020072
9. *Chalikov D.*, *Babanin A.V.* Parameterization of wave boundary layer // Atmosphere. 2019. Vol. 10, Iss. 11: 686. doi: 10.3390/atmos10110686
10. *Monin A.S.*, *Yaglom A.M.* Statistical fluid mechanics: mechanics of turbulence. Cambridge: M.I.T. Press., 1971. 770 p. doi: 10.1119/1.10870
11. *Miles J.W.* On the generation of surface waves by shearflows // Journal of Fluid Mechanics. 1957. Vol. 3, Iss. 2. P. 185–204.
12. *Hasselmann K.*, *Barnett R.P.*, *Bouws E.* et al. Measurements of wind-wave growth and swell decay during the Joint Sea Wave Project (JONSWAP) // Technical Report. Deutches Hydrographisches Institute, 1973. 95 p.